International Journal of ChemTech Research
CODEN(USA): IJCRGG ISSN : 0974-4290
Vol.6, No.1, pp 691-704, Jan-March 2014

Slurry Erosion Resistance of Laser-modified 16Cr–5Ni Stainless Steel

S. Sathik Basha[1]*, V.M. Periasamy[2], M. Kamaraj[3]

[1]Department of Physics, B.S. Abdur Rahman University, Chennai, India,
[2]B.S. Abdur Rahman University, Chennai, India,
[3]Department of Metallurgical and Materials Engineering, IIT Madras, India.

*Corres. author: sathik_sb@yahoo.co.in,
Tel.no.919444226819

Abstract: To enhance erosion resistance of 16Cr–5Ni steel surface for use in hydroturbine applications, surface hardening study was carried out using a high-power fiber coupled diode laser. For laser surface alloying (LSA), Wallex-50 powder was coated onto 16Cr–5Ni steel surface (two-stage process) before subjecting the surface to laser treatment and then laser treated to enhance the surface roughness. Characterization of laser-treated and untreated surfaces was analyzed by X-ray diffraction, optical microscopy, scanning electron microscopy and Vickers microhardness tests. Microhardness profile across the cross-section of a laser-modified hardened sample showed higher microhardness compared to the as-received 16Cr–5Ni steel specimen. Erosion resistance of the modified surface of the steel specimens was estimated through slurry erosion test for 1 h at two slurry velocities, 10 and 12 m/s, and three impingement angles, 30°, 60° and 90°. According to SEM images, the wear rate of laser-modified 16Cr–5Ni steel was found to be much lesser compared to the as-received steel specimen.
Keywords: 16Cr–5Ni martensite stainless steel; LSA; Wallex-50; microhardness; slurry erosion, wear analysis.

1. Introduction

Laser-assisted material processing [1, 2] has become a preferred technique for surface treatment due to the rapid development in the field of laser science and technology. Laser surface treatments have been known to enhance surface hardening; improve fatigue, erosion and corrosion resistance; and prevent stress corrosion and cracking of metals and alloys more efficiently compared to conventional methods [1–4]. In laser hardening, low-energy heat is applied on discrete surface regions to allow hardening to occur through self-quenching. No external quenching medium is required. Due to the application of low-energy heat, minimal distortion shall arise on the surface.

Low-carbon 16Cr–5Ni martensitic stainless steel (S+C 4405) is generally used in hydroturbines and water pumps due to its good corrosion resistance and weldability, excellent ductility, and low inclination to

crack on hardening [5]. However, the excessive solid particles entrained in water in hydroturbine application will subject this material to erosive wear and damage, thereby reducing the efficiency of turbines and ultimately causing their breakdown [6,7]. The damage due to the erosion can be reduced by surface modification techniques to improve the surface behaviour without affecting the bulk properties. Over the years, several surface modification techniques have been tried to improve either liquid impact erosion or solid particle erosion individually or simultaneously [8–10]. Of these, the laser-based surface modification techniques have been found to provide superior surface layers with distinct microstructures and compositions.

One of the best known methods for surface hardening is laser surface alloying (LSA). In this method, the surface is first coated with an alloy and then hardened by laser treatment, thereby improving corrosion, erosion, and wear resistances of the surface [11,12]. Erosion wear studies on 16Cr-5Ni martensite stainless steel were rarely reported.

In this study, the erosion wear resistance of laser-modified surface of low-carbon 16Cr–5Ni martensitic stainless steel has been investigated. The secondary phases of samples were examined by the X-ray diffraction pattern. The microstructures of the top and cross-sections were investigated using optical and scanning electron microscopy. Microhardness and wear studies have been evaluated and discussed. Erosion tests on the substrate and coating deposits were performed using a slurry jet erosion test rig (ASTM G73 standard) by varying slurry velocity and impingement angle. Erosion behaviour of as-received and LSA-treated samples was analyzed using the SEM.

2. Experimental

2.1. Materials And Surface Modification

Plates of 16Cr–5Ni martensitic stainless steel of size 20×20×7 mm were used as the base material (substrate) and Wallex-50 powder (Co based hard powder) was chosen as the coating material in the experimental study. Chemical compositions and hardness values of 16Cr–5Ni steel and Wallex-50 powder are shown in Table 1.

For slurry experiments, white silica powder of particle size 200 µm was used as erodent particle. The morphology of silica powder shown in Fig.1 reveals that the silica particles have sharp edges.

Next, Surface of the substrate material was prepared to be hardened by laser surface alloying (LSA) method. The green precursor (Wallex-50) mixed with polyvinyl acetate solution was coated to a thickness of 0.7–0.9 mm on to as-received steel. A fiber-coupled diode laser (model LDF 6000) at wavelength 915–980 nm, beam size 17 × 2 mm, and working distance 135 mm was used to treat the coated surface. Laser scanning speed was maintained between 10 and 15 mm/s and laser power density was set between 2500 and 4500 W/cm^2. For LSA, a depth of deposit of 0.35–0.46 mm could be easily achieved at a single pass.

Table 1 . Chemical composition (wt.%) and hardness profile of the substrate and the deposit

Material	C	B	Si	Cr	W	Mo	Mn	Co	Ni	Fe	Hardness, (HV)
16Cr–5Ni steel	0.058	—	1.00	16	—	0.50	1.00	—	5	Balance	380–392
Wallex-50	0.8	3.4	2.75	19	10.00	—	—	Balance	18.00	1.00	830–859

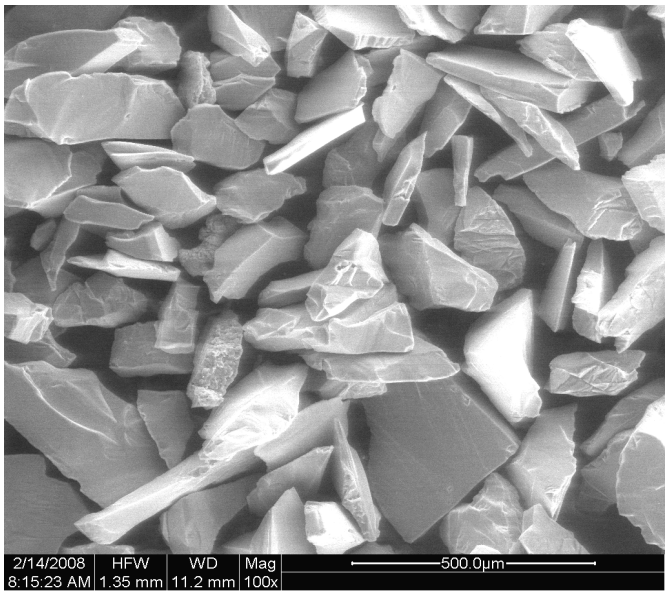

Fig.1. SEM image of silica powder of average particle size 200 µm

2.2. Slurry Erosion Wear Tests

Before the erosion test, the as-received and laser-treated samples were machined and polished with alumina to achieve a surface finish equal to 1 µm. Then, the samples were thoroughly cleaned with acetone and water to remove surface contaminations and then dried. A slurry jet erosion test rig (ASTM G73) was employed to study the erosion wear behaviour of the samples. Silica mixed with water was used as slurry. White silica sand particles of average size 200 µm were used as an erodent and the hardness of the erodent was 1100 VHN. Wear test was carried at slurry flow velocity of 10 and 12 m/s at three impingement angles 30°, 60° and 90°. Slurry concentrations of 10 and 15 kg/m^3 were applied for the wear test. Nozzle to sample distance and nozzle diameter were 50 mm and 6 mm, respectively. The duration of erosion test was 1 h. The test facility consists of a conical vessel of 10 liters capacity in which to mix the slurry. The holder in which the samples were kept had a provision to vary the angle of the sample with respect to the jet. Slurry was pumped through the impeller system and directed at the sample via the nozzle. Flow of the slurry was controlled by a motor. Erosion was determined using the weight loss method. The details of slurry erosive wear test facility can be found elsewhere. [11].

During slurry erosion test, blunting of particles could result from continuous impact of slurry particles with the test surface. To avoid this, the slurry was replaced every 30 minutes for all tests. Slurry erosion tests were performed under well-controlled test conditions (Table 2).

Effect of slurry particle velocity and impingement angle of the particle on surface erosion was investigated. A precision balance with accuracy to 0.01 mg was used to measure the cumulative loss of mass at regular intervals.

Table 2. Details of slurry erosion test

Target materials	Erodent size	Variable test parameters
Substrate (16Cr-5Ni steel) Wallex-50 deposit	200 µm	Velocity: 10, 12 m/s Angle of impingement: 30°, 60°, 90° Slurry concentration: 10, 15 kg/m^3

3. Results and Discussion

3.1. XRD Analysis

The XRD patterns of as-received and laser-treated samples were obtained using Cu-K_α radiation in order to identify their secondary phases and are shown in (Fig. 2). For the as-received sample (Fig. 2a), the phases identified were α-$Cr_{0.03}Fe_{0.97}$, α-$Fe_{10.8}Ni$ and $Cr_{1.36}Fe_{0.52}$ and represented low-carbon lath-type martensite. For laser-treated sample (i.e., laser-modified deposits), the XRD pattern (Fig. 2b) revealed the presence of secondary phases such as CoCx**,** α-$CoFe_{15.7}$ and Co_2C, suggesting that the surface was rich in cobalt.

3.2. Microstructural and Coating Characteristics

For microstructural studies, the surfaces of the as-received sample and laser-treated sample required to be metallographically polished and etched with Villela's reagent. Briefly, surfaces of the samples were polished using water emery sheets followed by fine polishing with alumina and diamond paste and then etching. The microstructures of the samples as revealed by SEM images are seen in Fig. 3.

The microstructure of 16Cr–5Ni steel (Fig. 3a) consisted of low-carbon tempered martensite with small amounts of δ-ferrite and finely dispersed austenite, suggesting that the structure should have superior toughness. Whereas, the microstructure of Wallex-50-coated steel (Fig. 3b) possessed a higher solid solution matrix of Co, C and W (Table 1), recognized as a needle of alpha solid solution distributed in beta solid solution throughout. It also revealed interdendritic alloy carbide in cobalt solid solution.

The coating parameters were found by calculating the height, depth, width and thickness of coating (Fig.4 and Table 3). The dilution ratio measured for LSA of Wallex-50 deposit was more than 50% for all samples. The appreciable level of dilution as a result of laser cladding was 8–10%. The dilution rate of laser deposits reported in this study has been exceptional.

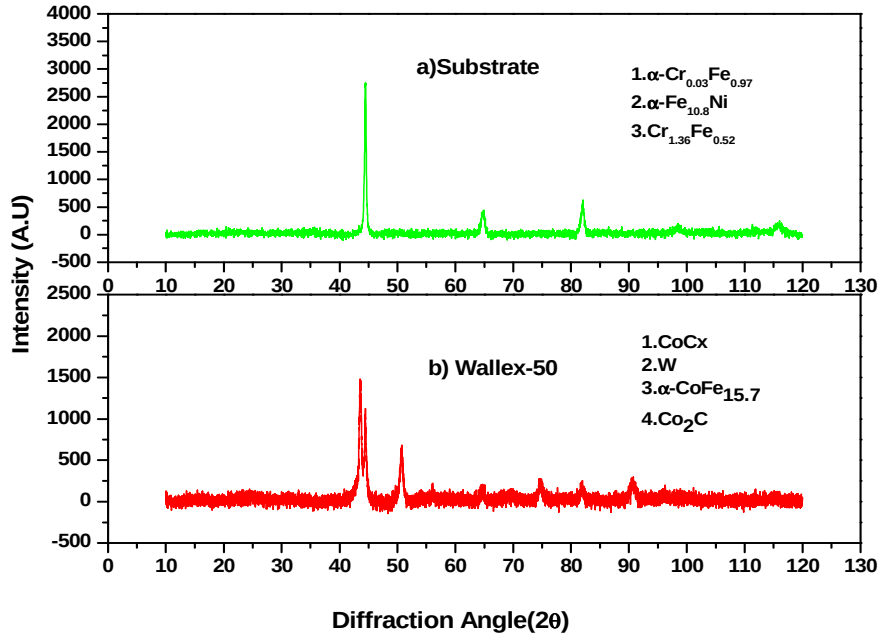

Fig.2. XRD patterns of (a) substrate (16Cr-5Ni steel) and (b) Wallex-50 deposit

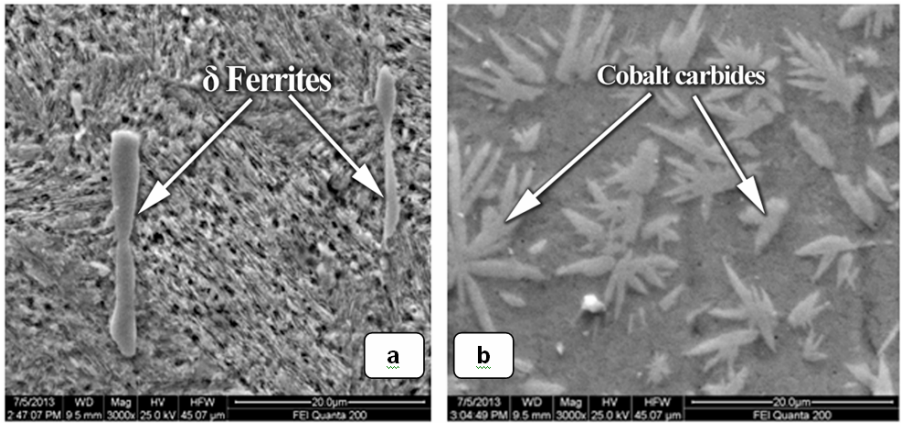

Fig.3. SEM image showing the microstructures of (a) 16Cr–5Ni steel and (b) Wallex-50 deposit

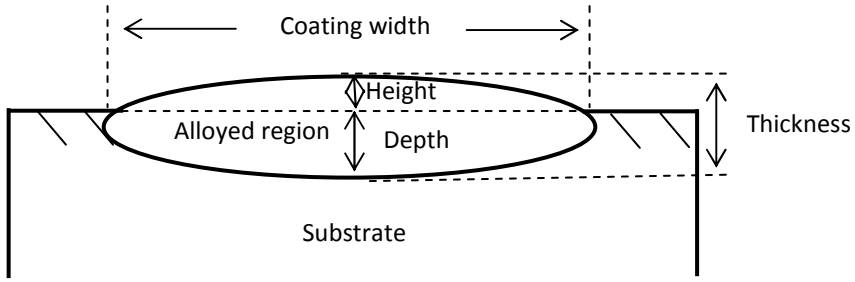

Fig.4. Schematic of LSA characteristics.

Table 3. Characteristics of LSA coating

Coatings	Coating characteristics			
	Height, a (mm)	**Depth, b (mm)**	**Thickness, a+b (mm)**	**Dilution, [b/(a+b)]x100 (%)**
Wallex-50	0.35	0.45	0.8	56.25

Figure 5 shows the SEM images of the cross-sectional view of laser deposit on the substrate, suggesting excellent distribution of the coating as well as good metallurgical bonding between the deposit and the substrate. The micrograph also reveals the laser-melted zone. A non-homogeneous microstructure of the laser-melted zone was because of both a great undulation of liquid alloy composition and differences of solidification rate in local areas. The composition supercooling at the interface had the least value owing to both the lower temperature of the matrix and the higher temperature gradient at the liquid–solid interface, causing the liquid–solid interface to grow slowly during solidification and thus exhibit epitaxial solidification growth.

3.3. Interface Analysis

The interface between the deposit and the substrate surface was studied by line scanning method (Fig. 6) using a high-resolution scanning electron microscope, suggesting a visibly good interface between the deposit and substrate. The results of line scan across the interface show the distribution of elements as count versus distance along with secondary phases. The SEM image has two parts, the left corresponding to the laser-treated region and the right corresponding to the substrate region.

The interface analysis suggests that the main elements of the deposit were Co, W, C and Cr, forming secondary phases such as CoCx, α-$CoFe_{15.7}$,W and Co_2C. At the substrate region, Co, Ni and W were decreased while Fe was increased. But C and Cr have been distributed uniformly at deposit and substrate regions.

3.4. Microhardness Studies

Hardness determines how much resistance against corrosion the coating will provide to the substrate. The higher the hardness, the higher will be the erosion resistance. The microhardness profiles measured across the interfaces of the substrate and the deposit are presented in Fig. 7.

The figures reveal three regions, namely substrate, heat-affected zone (HAZ) and the laser-treated region. From Fig. 7, it is seen that the maximum microhardness was about 850 HV at a depth of 0.1 mm. The maximum microhardness was seen up to 0.25 mm from the top surface for Wallex-50. Hardness decreased gradually in the HAZ from 720 HV to 680 HV at a depth of 0.46–0.62 mm. Thereafter, the hardness profile of laser-treated sample has reduced to the level of as-received sample. The hardness of the as-received sample was 380–392 HV (Table.1).

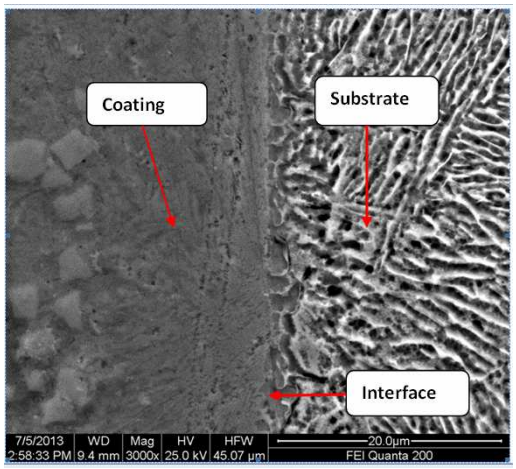

Fig.5. SEM microstructure of laser-treated Wallex-50-coated steel (cross-sectional view)

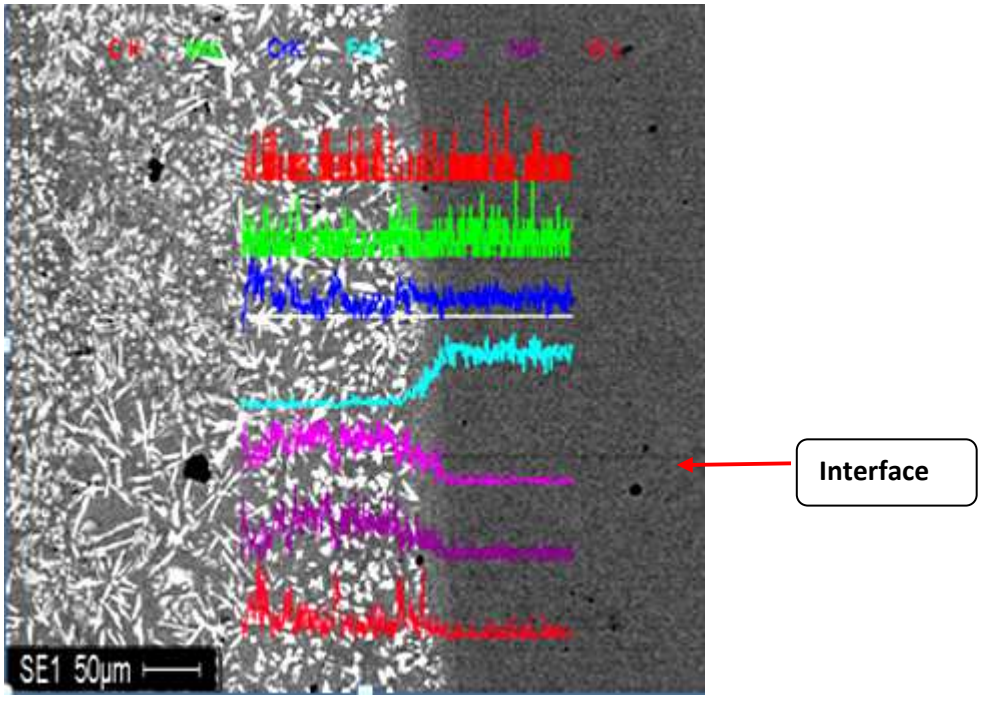

Fig.6. Interface element analysis of laser-treated Wallex-50 coated steel

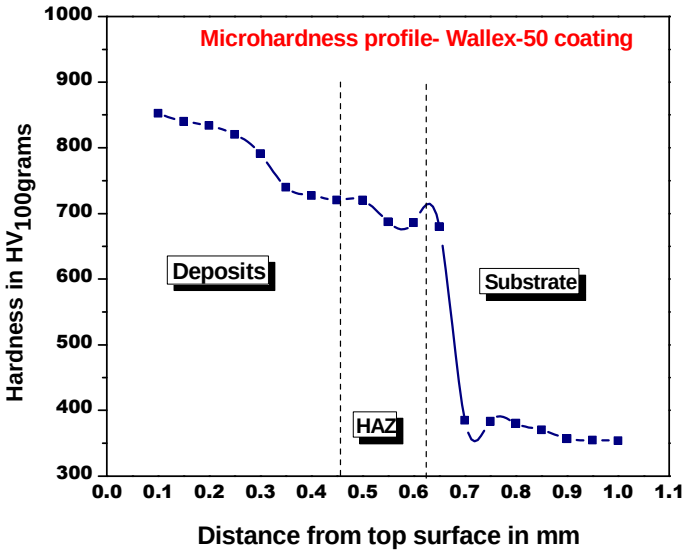

Fig.7. Microhardness profile of laser-treated Wallex-50-coated steel

3.5. Wear Analysis

3.5.1. Cumulative Mass Loss

Erosion during slurry test was measured in terms of cumulative mass loss. In Fig. 8(a,b) is shown the cumulative mass loss after 1 h of erosion test at 30^{o} for slurry concentrations 10 and 15 kg/m^{3} and slurry velocities 10 and 12 m/s for the laser-treated surface. In hydroturbines, slurry particles impinge mostly at a low angle, and so mass loss at a low angle of impingement (30^{o}) was considered in this study. The laser-treated surface exhibited better performance over 16Cr–5Ni steel for all slurry test conditions. Mass loss of all target materials was very less at initial stages (incubation period). A drastic increase in mass loss was observed after 10 minutes of exposure of slurry for all target materials and at velocities 10 and 12 m/s. Figure 9(a,b) compares cumulative mass loss for 1 h of slurry flow at two different velocities (10 and 12m/s) and slurry concentrations (10 and 15 kg/m^{3}). Mass loss was found to increase with slurry velocity and slurry concentration. In Fig. 9a, it is seen that the mass of loss reduced by ~3.03-fold at 10 m/s and by ~2-fold at 12 m/s for laser-treated sample as compared with the substrate for a slurry concentration of 10 kg/m^{3} . Similarly, in Fig. 9b, the mass of loss reduced by ~1.55-fold at 10 m/s and by ~1.2-fold at 12 m/s for laser-treated sample as compared with the substrate for a slurry concentration of 15 kg/m^{3}. The reduction in mass loss for laser-treated sample was due to its higher microhardness compared to the substrate, as well as due to the dispersion of hard secondary phases within the microstructures, providing these deposits with excellent resistivity to abrasive wear.

3.5.2 Erosion Rate Plot

Impact angle and impact velocity of the erodent are the two main parameters that influence wear rate and surface degradation in turbine parts [13]. Impact angle may be defined as the angle between the target surface and the direction of striking velocity of the solid particle. To study the effect of impact angle on erosion is the most sensitive way to understanding the mechanism of erosion and quantum of erosion. The variation of erosion wear with impact angle depends on whether the target surface material is of brittle or ductile type. It has been found that the maximum erosion rate for a ductile-type material is at impingement angle of approximately 20–30°, and erosion rate would decrease at higher angles [14-17]. Whereas for a material of brittle type, the rate of erosion will rise steadily with angle, reaching a peak at 90^{o} [16]. In the present work, erosion rate was measured during 1 h slurry test for impingement angles 30°, 60° and 90° and slurry velocity 10 and 12 m/s (Fig. 10). The mode of erosion was detected from the erosion rate. Erosion rate was determined from cumulative mass loss. The laser-treated deposit showed lower erosion rate compared with the substrate (Fig. 10) for all impingement angles and slurry velocities. The substrate showed a mixed (ductile and brittle) type of erosion behavior at 12

m/s (Fig. 10b), whereas at 10 m/s, the erosion behaviour of ductile type was noted (Fig 10a). It is known that 16Cr–5Ni presents a mixed structure of martensite, γ_R (retained austenite) and δ-ferrite at room temperature after tempering. The superior toughness of this structure is believed to be due to retained austenite [5]. The erosion behavior of Wallex-50 deposit was that of ductile type at velocity 12 m/s because the erosive wear was high at 30° and low at 90°, whereas at 10 m/s, the erosion behavior was of mixed type. It is the slurry velocity that determines the energy of the erodent particle and hence the erosion rate. Figure 10 shows that as particle velocity increases, the erosion rate tends to increase. The laser-treated samples showed low erosion rate due to the presence of hard secondary phases and carbides. It is to be noted that at velocity 12 m/s, the erosion rate was low at 60° as compared with that at 30° and 90° for both samples.

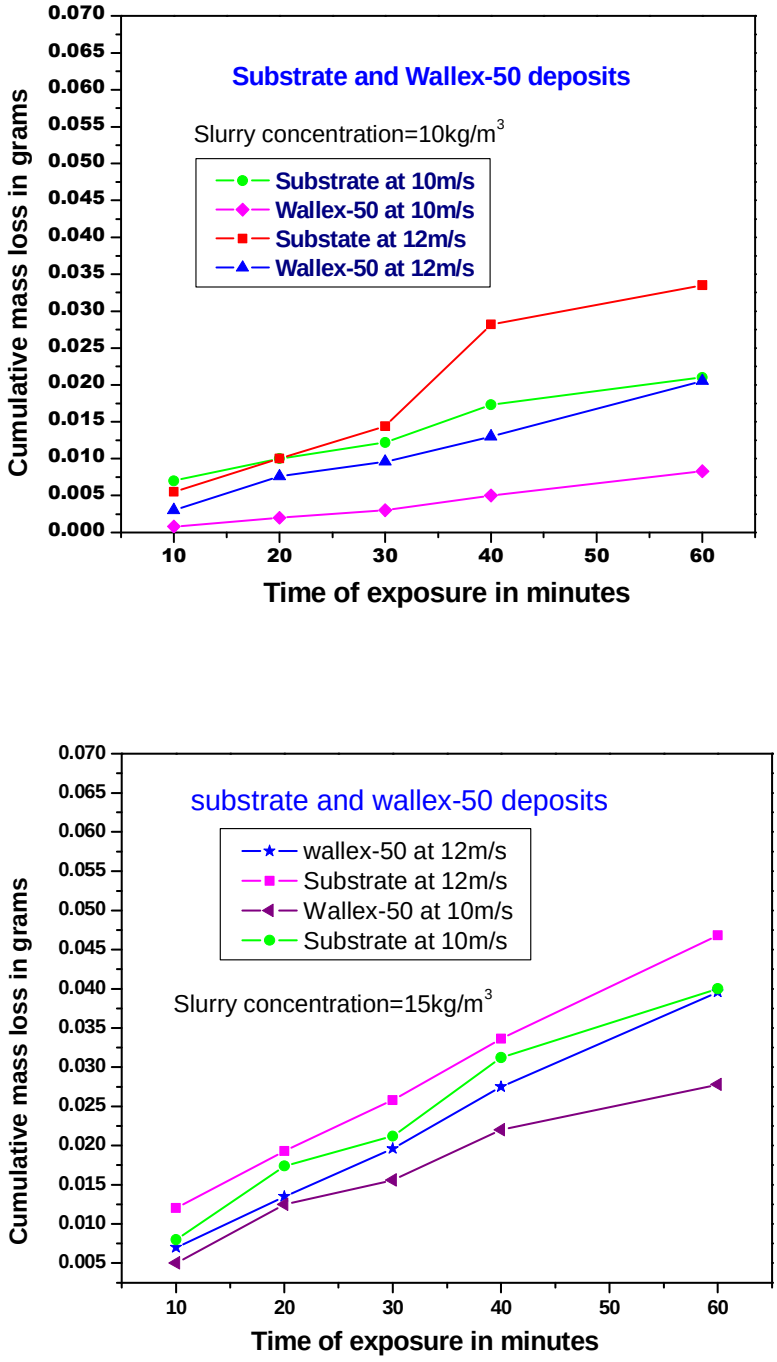

Fig.8.(a,b) Cumulative mass loss as a function of time at 30° impingement angle and slurry concentrations 10 and 15 kg/m^3

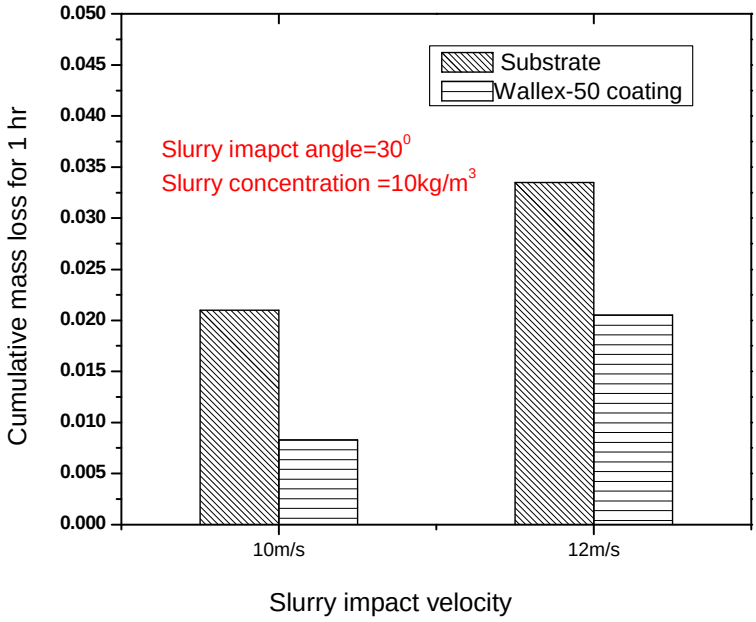

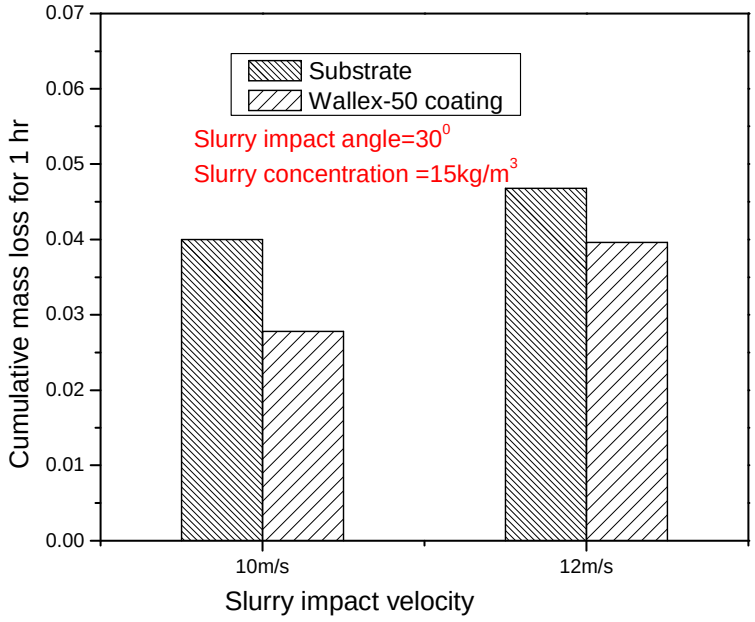

Fig.9.(a,b) Histogram representation of mass loss of coated and substrate samples at slurry concentrations 10 and 15 kg/m^3

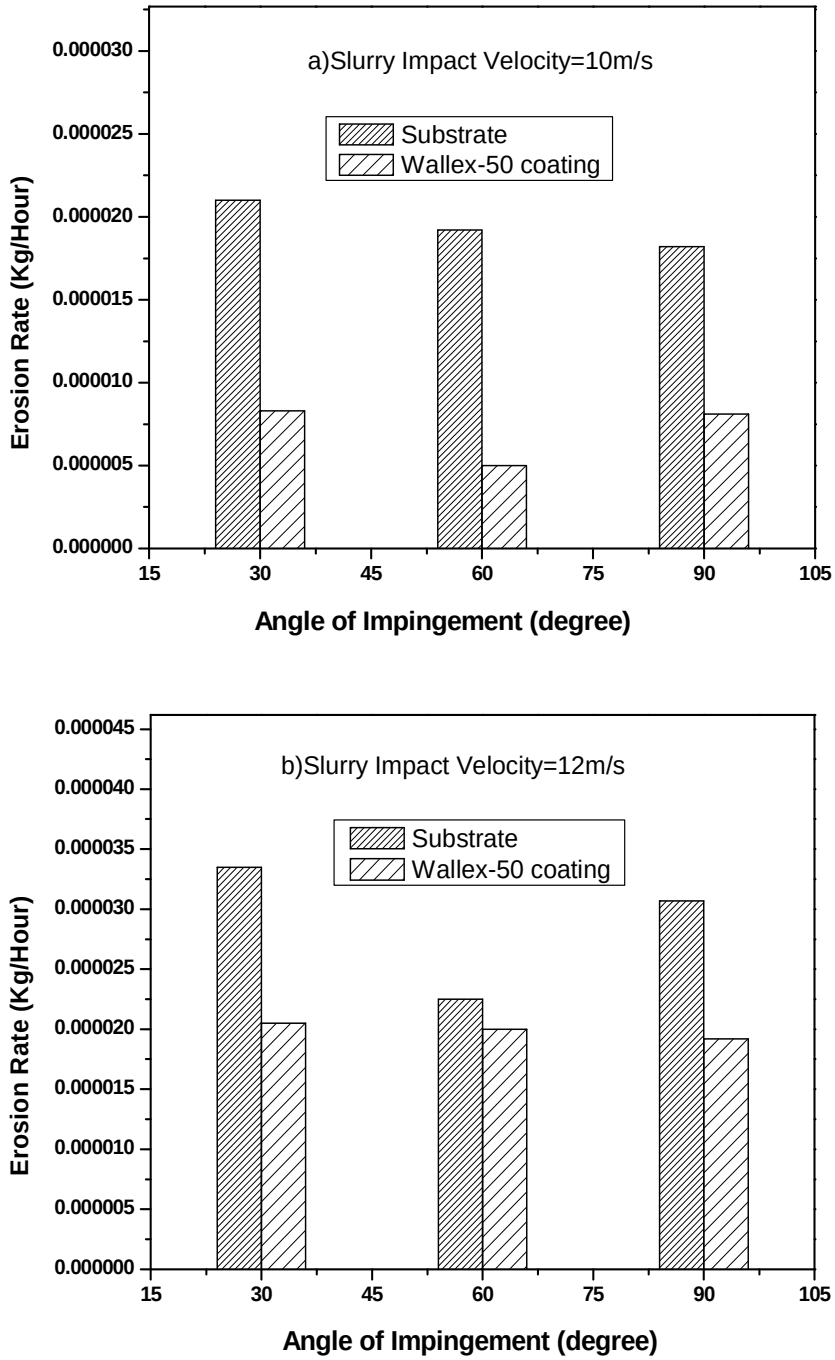

Fig. 10 (a,b) Erosion rate as a function of impingement angle for 1 h slurry test at velocity of (a) 10 m/s and (b) 12 m/s.

3.6. Wear Analysis

Several erosion wear mechanisms such as cutting, ploughing, plastic deformation and cracking are known. Ductile and brittle materials differ in their erosion wear mechanism. Cutting wear occurs when a hard particle cuts through a soft target material. Here, the impacting particle comes into contact with the target material at a low angle and cuts a chip off it. Thus, the shape of the impinging particle is the main factor in cutting wear. Angular-shaped impinging particles are known to produce higher wear. Ploughing wear takes place when a spherical particle hits on the target material at a large rack angle. In ploughing wear, material removal is usually lesser. Plastic deformation occurs when a spherical particle collides on a target surface at a high velocity,

leading to crater and crack formation, which often results in wear by brittle fracture. In plastic deformation, an extruded shear lip will usually form, which may fall off by fatigue caused by continuous impact.

Erosion performance of as-received and laser-treated samples was analyzed using their SEM images. The mechanism of material removal by erosion largely seemed to depend on material property and impingement angle. Generally, plastic deformation and cutting were the erosion mechanisms identified to be associated with material removal in the present study. Ductile materials usually undergo volume loss by direct microcutting or plastic deformation, followed by cutting. In brittle materials, the continuous particle impact and energy transfer associated with it often result in fatigue. SEM images of erosion wear by silica particles of average size 200 μm at slurry velocity 12 m/s, slurry concentration 10 kg/m^3 and impingement angles 30°, 60° and 90° are shown in Fig. 11, 12 and 13, respectively, for the as-received and laser-treated samples. .

The SEM images of the eroded surfaces of the as received sample and the laser treated Wallex-50 coated sample for 30° angle of impingement are shown in Fig. 11(a) and 11(b) respectively. It is observed from the SEM (Fig. 11a) of the as-received 16Cr–5Ni steel, under a low angle of impact (30°), chip formation and microcutting were the chief erosion mechanisms involved, due to the oblique shear force imparted by the erodent, a characteristic typical for a ductile material. At the same impact angle for laser-treated surface, carbide intact and carbide fracture were seen at the impact region (Fig. 11b), suggesting that the wear was due to plastic deformation. Also, plastic deformation has resulted in lesser amount of material wear from laser-treated surface, in contrast to the substrate material. Therefore, a clear reduction in cumulative mass loss as well as erosion rate was seen in laser-treated surface at slurry velocity of 12 m/s compared with the as-received material. Moreover, at different durations of slurry erosion, such as 10, 20, 30, 40, 50 and 60 min (at 12 m/s), the quantum of material removal was lesser for laser-treated surface compared with the as-received sample (Fig.8a).

Figure 12 shows the erosion mechanism for samples at an impingement angle of 90°, wherein the surface of the substrate appears weak due to fatigue and develops cracks due to continuous impact. The substrate reveals a mixed mode of erosion behaviour, whereby crater, crater lips and cutting action were the main mechanisms of material removal involved (Fig. 12a). We understood that strain hardening and embrittlement caused erosion on the surface in as-received samples [11]. Even at normal impinging angles, the stress that develops will accumulate and cause damage due to microforging and extrusions, resulting in crater and crater lips. It is noteworthy that, even at an impinging angle of 90°, the erosion rate of laser-treated sample was almost half that of the as-received sample (Fig. 10b). For the laser-treated surface (Fig. 12b), we understood that pullout of particles was the main wear mechanism involved, in that the surface at first gets plastically deformed to form flakes around the striking point. Thereafter, repeated strikes on the flakes will lead only to particle pullout.

Figure 13(a,b) shows the erosion mechanism of the as-received and laser-treated samples at impingement angle of 60°. For both samples, the topography of eroded surfaces reveals the presence of ploughs formed due to the extrusion of platelets at the impact zone. Ploughing and plough lips have been thought to result in lesser erosion on the surface. As seen in the histogram (Fig. 10b), the erosion rate was lesser at 60° than at 30° and 90° for the as-received sample, whereas for the laser-treated sample, erosion at 60° suggests a ductile mode (Fig. 10b). Figure 13a shows that the ploughs in 16Cr–5Ni steel are much wider than in laser-treated sample, suggesting higher material removal in the former. This is also evident from the erosion rate plots showing that the erosion rate was higher for the as-received sample compared with the laser-treated sample at 60^o. In conclusion, the results of the present study throw light on the fact that laser-modified Wallex-50-coated 16Cr–5Ni steel possesses twice as much erosion resistance as 16Cr–5Ni steel, potentially enhancing the life time of 16Cr–5Ni steel used in turbine applications.

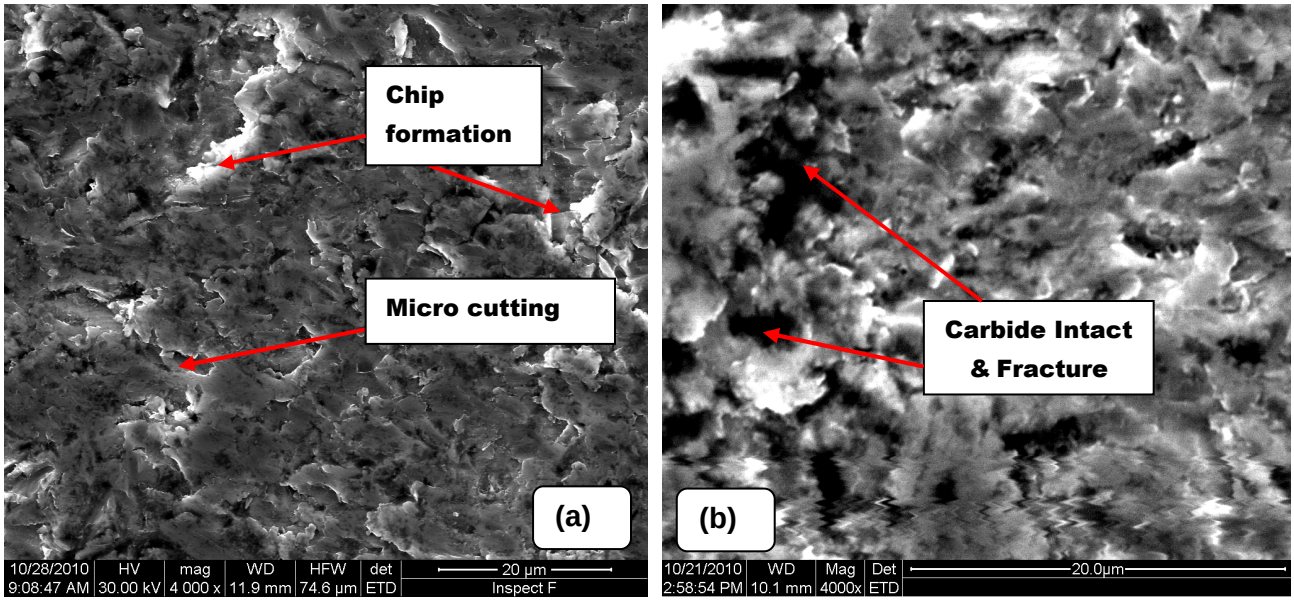

Fig.11. SEM image of slurry-eroded surface of (a) 16Cr–5Ni steel and (b) laser-treated Wallex-50-coated steel at an impingement angle of 30°.

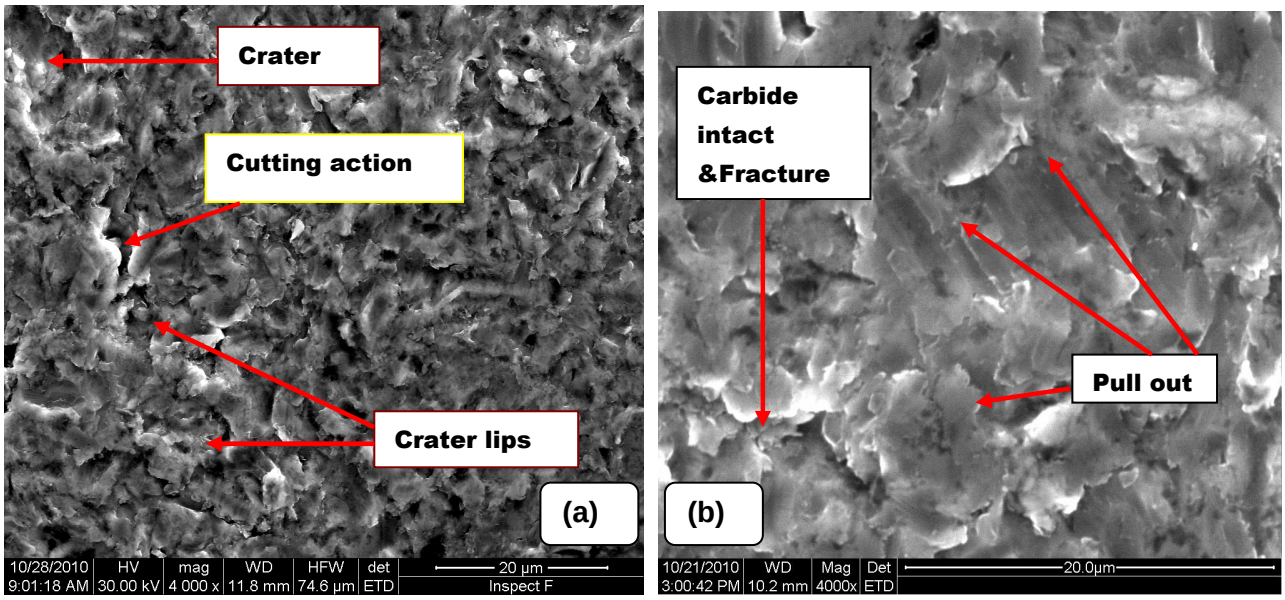

Fig.12. SEM image of slurry-eroded surface of (a) 16Cr–5Ni steel and (b) laser-treated Wallex-50-coated steel at an impingement angle of 90°.

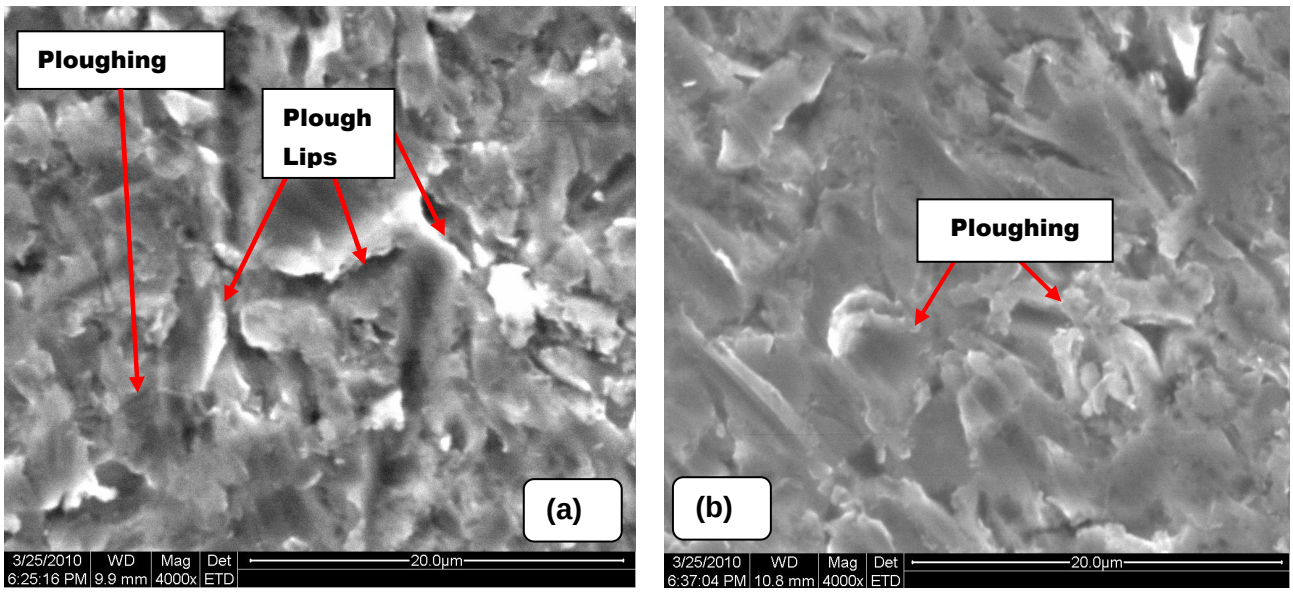

Fig.13. SEM image of slurry-eroded surface of (a) 16Cr-5Ni steel and (b) laser-treated Wallex-50-coated steel at an impingement angle of 60°.

4. Conclusions

In the present study, laser hardening of 16Cr–5Ni steel was performed using fiber-coupled diode laser at a single pass. Microhardness of Wallex-50 is ~850 HV and is ~2.2 times that of 16Cr–5Ni steel. From erosion tests, the cumulative volume of loss for laser-treated 16Cr–5Ni steel was lesser than that of as-received 16Cr–5Ni steel for all impingement angles and all velocities studied. For the laser-treated sample, the volume of loss reduced by ~3.03-fold at 10 m/s, and at 12 m/s, the volume of loss reduced by ~2-fold, compared with the as-received sample.

At 12 m/s, the substrate showed a mixed (ductile and brittle) type of erosion behaviour, whereas at 10 m/s, the erosion behaviour was of ductile type. On the other hand, the erosion behaviour of laser-treated sample showed a mixed type of erosion behaviour at 10 m/s and a ductile type of behaviour at 12 m/s. Interestingly, erosion wear in laser-treated sample was lesser compared with the as-received sample due to the improved microhardness in the former due to laser treatment. Thus, it is experimentally shown that laser-modified, Wallex-50-coated 16Cr–5Ni steel is twice as erosion-resistant as 16Cr–5Ni steel. Our finding is valuable in the processing of 16Cr–5Ni steel for turbine applications.

Acknowledgements

The present work was supported and carried out by Indian Institute of Technology Madras (IIT-M), India. Laser coating on 16Cr–5Ni steel was performed at ARCI, Hyderabad, India. We thank both IIT-M and ARCI.

References

[1] Mordike,B.L., Lasers in materials processing, ProgMaterSci.42 (1997), 357–372.

[2] Schaaf.P., Laser Nitriding of Metals, ProgMaterSci.47 (2002), 1–161.

[3] Kruusing.A., Underwater and water-assisted laser processing:Part 1—general features, steam cleaning and shock processing,Optics and Lasers in Engineering.41(2004),307–327.

[4] Kalainathan.S., Sathyajith.S., Swaroop.S., Effect of laser shot peening without coating on the surface properties and corrosion behavior of 316L steel,Optics and Lasers in Engineering. 50 (2012),1740–1745.

[5] Niederau.H.J.: A New Low-Carbon 16Cr-5Ni Stainless Martensitic Cast Steel, Stainless Steel Casting, a symposium sponsored by ASTM Committee (1980), pp.382-393.

[6] Padhy.M.K., Saini.R.P., Effect of size and concentration of silt particles on erosion of Pelton turbine buckets, Energy. 34 (2009), 1477–1483.

[7] Chauhan.A.K., Goel.D.B., Satya Prakash, Erosion behaviour of hydro turbine steels, Bull. Mater. Sci. 31 (2008) ,115–120.

[8] Bose.K., Wood.R.J.K., Wheeler.D.W., High energy solid particle erosion mechanisms of super hard CVD coatings,Wear.259 (2005) ,135-144.

[9] Höppel.H.W., Mughrabi.H., Sockel.H.G., Schmidt.S. ,Vetter.G., Hydroabrasive wear behaviour and damage mechanisms of different hard coatings, Wear (1999), 1088-1099.

[10] Zhang.D., Zhang.X., Laser cladding of stainless steel with Ni–Cr3C2 and Ni–WC for improving erosive–corrosive wear performance,Surface and Coatings Technology. 190 (2005), 212-217.

[11] Shivamurthy.R.C., Kamaraj.M., Nagarajan.R., Shariff.S.M., Padmanabham.G., Influence of microstructure on slurry erosive wear characteristics of laser surface alloyed 13Cr–4Ni steel, Wear. 267 (2009) 204–212.

[12] Tucker.T.R., Clauer.A.H., Wright.I.G., Stropki.J.T., Laser-processed composite metal cladding for slurry erosion resistance,Thin Solid Films, 118 (1984), 73– 84.

[13] Lopez.D,, Congot.J.P,, Cano.J.R,, Toro.A,, Tschiptschin.A.P,, Effect of particle velocity and impact angle on the corrosion–erosion of AISI 304 and AISI 420 stainless steels, Wear. 259 (2005), 118-124.

[14] Oka.Y.I., Okamura.K., Yoshida.T., Practical estimation of erosion damage caused by solid particle impact, Part 1: Effects of impact parameters on a predictive equation, Wear .259 (2005), 95-101.

[15] Clark.H.M., Wong.K.K., Impact Angle Particle Energy and Mass Loss in Erosion by Dilute Slurry, Wear. 186 (1995) 454–464.

[16] Stachowiak.G.W., Particle angularity and its relationship to abrasive and erosive wear, Wear .241 (2000) 214-219.

[17] Wheeler.D.W., Wood.R.J.K., Erosion of hard surface coatings for use in offshore gate valves, Wear, Vol. 258 (2005), pp. 526–536,Wear. 258 (2005) 526-536.

*****